

Adaptive Stabilization of Thermoacoustic Oscillations in a Rijke Tube

Juan Paredes, Syed Aseem Ul Islam, and Dennis S. Bernstein

Abstract—Thermoacoustic systems are self-oscillating due to the fact that a constant input (fuel rate in gas turbine combustors for example) yields an asymptotically oscillatory response. This behavior arises due to the interaction between combustion and acoustics, resulting in thermoacoustic oscillations. This paper provides a numerical and experimental investigation of retrospective cost adaptive control (RCAC) for adaptively suppressing thermoacoustic oscillations under sampled-data control.

I. INTRODUCTION

The destruction of the Tacoma-Narrows bridge in 1940 after little more than four months of operation provides a graphic illustration of a self-oscillating system (SOS), that is, a system for which a constant input produces an oscillatory response. SOS arise in biochemical systems, aeroelasticity, and combustion [1]–[10]. Although the classical example of a SOS is the van der Pol oscillator, SOS may have an arbitrary number of states and need not possess a limit cycle. Control of SOS has attracted substantial interest motivated by diverse applications [11]–[16].

The goal of the present paper is to investigate the performance of an adaptive controller for suppressing oscillations in a Rijke-tube model and validate these results in a Rijke-tube experiment. A Rijke tube is a spatially one-dimensional thermoacoustic system that is highly susceptible to thermoacoustic oscillation [17]–[22]. Experimental applications of various control algorithms are reported in [23]–[25].

In the present paper, a 1D nonlinear Rijke-tube model and a Rijke-tube experiment are used to investigate adaptive stabilization in a sampled-data setting using retrospective cost adaptive control (RCAC) [26]. This technique was applied to the van der Pol oscillator in [26] and to models of scramjet combustors in [27] and [28], which exhibit thermoacoustic oscillations. The numerical investigation in the present paper is based on a 1D nonlinear Rijke-tube model derived from [29]–[31]. The model parameters are chosen so that the model response is similar to that of the Rijke-tube experiment built in the University of Michigan laboratory. This model features a linear map, time delays, asymptotically stable linear dynamics, and a continuous, bounded nonlinearity.

The goal of the present paper is to determine the modeling information required by RCAC to suppress thermoacoustic oscillations in the 1D nonlinear Rijke-tube model and a Rijke-tube experiment. The numerical investigation involves variations of the model parameters in order to determine the robustness of the modeling information required by RCAC,

while the physical tests are used to validate these results. The contribution of this paper is thus a numerical and experimental investigation of adaptive sampled-data stabilization of SES with application to a 1D nonlinear Rijke-tube model.

The contents of the paper are as follows. Section II presents the nonlinear Rijke-tube model. Section III describes the adaptive control law considered in this paper for adaptive stabilization. Section IV considers the approach under which the discrete-time adaptive controller interacts with the continuous-time models. Section V presents numerical examples in which the adaptive controller stabilizes the nonlinear model of the Rijke tube. The performance of the adaptive controller is compared against that of a continuous-time time-delayed integral controller. Section VI presents the setup of the Rijke-tube experiment built in the University of Michigan laboratory. Section VII presents experimental results in which the adaptive controller stabilizes the Rijke-tube experiment described in Section VI. Finally, Section VIII presents the conclusions of the paper.

II. NONLINEAR MODEL OF A RIJKE TUBE

The setup considered for the Rijke tube is displayed in Fig. 1, where a heating coil is placed inside a vertical tube x_d m below the top of the tube and x_u m above the bottom of the tube. Due to the heat produced by the coil, the air travelling through the heating zone expands and causes a local increase in pressure, which propagates along the tube and is fed back to the heating zone, which causes a thermoacoustic instability manifested as self-excited oscillations. In Fig. 1, f_1 and g_1 represent the acoustic pressure propagation in the upstream side, and f_2 and g_2 represent the acoustic pressure propagation in the downstream side. The objective is to suppress these thermoacoustic oscillations. For that purpose, a microphone is used to measure the pressure oscillations at x_{mic} m below the top of the tube, a speaker is placed below the tube as an actuator for oscillation suppression, and a digital controller is used to modulate the speaker pressure according to the pressure oscillation measurements from the microphone.

The nonlinear Rijke-tube model is based on the ducted flame model shown in [29] and derived in [30], [31]. Let $t \geq 0$ denote time, define $\mathbb{X} \triangleq [-x_u, x_d]$, and let $x \in \mathbb{X}$ denote a position within the tube in meters, where $x = 0$ m is the position of the heating coil in the tube. Let p and u be the airflow pressure and velocity, respectively, such that,

Juan Paredes, Syed Aseem Ul Islam, and Dennis S. Bernstein are with the Department of Aerospace Engineering, University of Michigan, Ann Arbor, MI, USA. {jparedes, aseemisl, dsbaero}@umich.edu

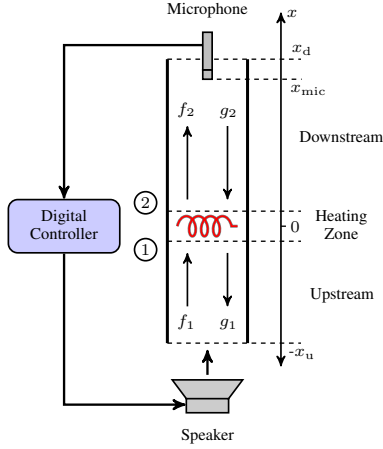


Fig. 1: Schematic of the Rijke tube.

for all $t \geq 0$ and $x \in \mathbb{X}$,

$$p(t, x) \triangleq \begin{cases} \bar{p}_1 + \tilde{p}_1(t, x), & x \in [-x_u, 0], \\ \bar{p}_2 + \tilde{p}_2(t, x), & x \in (0, x_d] \end{cases}, \quad (1)$$

$$u(t, x) \triangleq \begin{cases} \bar{u}_1 + \tilde{u}_1(t, x), & x \in [-x_u, 0], \\ \bar{u}_2 + \tilde{u}_2(t, x), & x \in (0, x_d] \end{cases}, \quad (2)$$

where $\bar{p}_1, \bar{p}_2 \in \mathbb{R}$ are the mean airflow pressure in the upstream and downstream sides, respectively, $\bar{u}_1, \bar{u}_2 \in \mathbb{R}$ are the mean airflow velocities in the upstream and downstream sides, respectively, and, for all $i \in \{1, 2\}$,

$$\tilde{p}_i(t, x) \triangleq f_i(t - \frac{x}{\bar{c}_i}) + g_i(t + \frac{x}{\bar{c}_i}), \quad (3)$$

$$\tilde{u}_i(t, x) \triangleq \frac{1}{\bar{\rho}_i \bar{c}_i} [f_i(t - \frac{x}{\bar{c}_i}) - g_i(t + \frac{x}{\bar{c}_i})], \quad (4)$$

where $\bar{c}_1, \bar{c}_2 \in \mathbb{R}$ are the mean wave speeds in the upstream and downstream sides, respectively, and $\bar{\rho}_1, \bar{\rho}_2 \in \mathbb{R}$ are the mean air densities in the upstream and downstream sides, respectively, f_1 and g_1 represent the acoustic pressure propagation in the upstream side, and f_2 and g_2 represent the acoustic pressure propagation in the downstream side. Furthermore, f_1 and g_2 are given by

$$f_1(t) \triangleq R_{us} g_1(t - \tau_u) + v(t - \frac{\tau_u}{2}), \quad (5)$$

$$g_2(t) \triangleq R_{ds} f_2(t - \tau_d), \quad (6)$$

where $R_{us}, R_{ds} \in \mathbb{R}$, $\tau_u \triangleq \frac{2x_u}{\bar{c}_1}$, $\tau_d \triangleq \frac{2x_d}{\bar{c}_2}$, and $v \in \mathbb{R}$ is the speaker pressure. Next, let the dynamics of the heat release rate of the coil Q be given by

$$b\dot{Q}(t) + Q(t) = a \text{sat}_{\bar{u}_1, \delta \bar{u}_1}(\bar{u}_1 + \tilde{u}_1(t, 0)), \quad (7)$$

where $a, b \in \mathbb{R}$, $\delta \bar{u}_1 \in [0, \bar{u}_1]$, and

$$\text{sat}_{\bar{u}_1, \delta \bar{u}_1}(u) \triangleq \begin{cases} \bar{u}_1 - \delta \bar{u}_1, & u < \bar{u}_1 - \delta \bar{u}_1 \\ u, & u \in [\bar{u}_1 - \delta \bar{u}_1, \bar{u}_1 + \delta \bar{u}_1] \\ \bar{u}_1 + \delta \bar{u}_1, & u > \bar{u}_1 + \delta \bar{u}_1 \end{cases}. \quad (8)$$

Let $\bar{Q} \in \mathbb{R}$ be the mean heat release rate of the coil and define $\tilde{Q}(t) \triangleq Q(t) - \bar{Q}$. Then, let $\mathcal{F}: \mathbb{R}^3 \rightarrow \mathbb{R}^2$ be a linear map such that

$$\begin{bmatrix} g_1(t) \\ f_2(t) \end{bmatrix} = \mathcal{F}(f_1(t), g_2(t), \tilde{Q}(t)) \triangleq X^{-1} \begin{bmatrix} Y & 0 \\ \frac{1}{A\bar{c}_1} \end{bmatrix} \begin{bmatrix} f_1(t) \\ g_2(t) \\ \tilde{Q}(t) \end{bmatrix}, \quad (9)$$

where $A \in \mathbb{R}$ is the tube cross-sectional area and $X, Y \in \mathbb{R}^{2 \times 2}$. Detailed expressions for X and Y are given in the appendix of [29]. Since the Mach numbers are low, X and Y are given by

$$X \triangleq \begin{bmatrix} -1 & 1 \\ \frac{1}{\bar{\gamma}-1} & \frac{\bar{c}_2}{\bar{c}_1} \frac{1}{\bar{\gamma}-1} \end{bmatrix}, \quad Y \triangleq \begin{bmatrix} 1 & -1 \\ \frac{1}{\bar{\gamma}-1} & \frac{\bar{c}_2}{\bar{c}_1} \frac{1}{\bar{\gamma}-1} \end{bmatrix}, \quad (10)$$

where $\bar{\gamma}$ is the adiabatic ratio of dry air at room temperature. Finally, define $\tau_{mic} \triangleq \frac{x_{mic}}{\bar{c}_2}$ and let \tilde{p}_{mic} be the acoustic pressure oscillations measured by the microphone such that

$$\begin{aligned} \tilde{p}_{mic}(t) &\triangleq \tilde{p}_2(t, x_{mic}) = f_2(t - \frac{x_{mic}}{\bar{c}_2}) + g_2(t + \frac{x_{mic}}{\bar{c}_2}) \\ &= f_2(t - \tau_{mic}) + R_{ds} f_2(t - (\tau_d - \tau_{mic})). \end{aligned} \quad (11)$$

The block diagram shown in Fig. 2 summarizes the dynamics of the nonlinear Rijke-tube model, where v is the speaker pressure and $y = \tilde{p}_{mic}$ is the microphone output. The model parameters used for the rest of the paper are shown in Table I. These were chosen to match the setup of the Rijke-tube experiment built in the University of Michigan laboratory and to match the response of the model to the response of the experiment. The open-loop responses ($v \equiv 0$) of the model and the experiment are displayed in Fig. 3 for 2 different positions of the heating element for comparison, which shows that the output of the model approximately matches the response of the actual system.

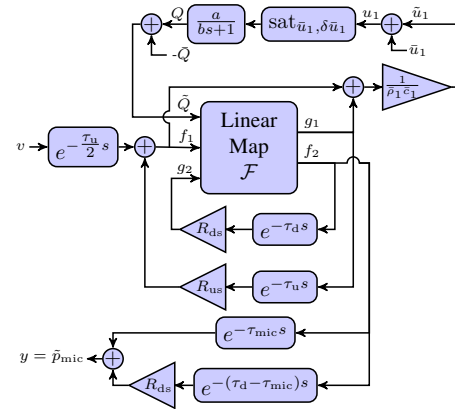


Fig. 2: Block diagram of the nonlinear Rijke-tube model. The control input is the speaker pressure v , and the measurement is the microphone output $y = \tilde{p}_{mic}$.

III. RETROSPECTIVE COST ADAPTIVE CONTROL

Consider the strictly proper input-output discrete-time (sampled) controller

$$u_k = \sum_{i=1}^{l_c} P_{i,k} u_{k-i} + \sum_{i=1}^{l_c} Q_{i,k} z_{k-i}, \quad (12)$$

TABLE I: Model Parameters for Numerical Examples

Parameter	Value	Units
R_{us}	-0.99	—
R_{ds}	-0.99	—
Q	150	W
\bar{c}_1	340	m/s
\bar{c}_2	360	m/s
$\bar{\rho}_1$	1.2	kg/m ³
\bar{u}_1	0.4	m/s
$\delta\bar{u}_1$	$5.2 \cdot 10^{-2}$	m/s
$\bar{\gamma}$	1.4	—
A	$4.6 \cdot 10^{-3}$	m ²
a	375	—
b	$2 \cdot 10^{-3}$	—
$\begin{bmatrix} x_d \\ x_u \end{bmatrix}$	$\begin{bmatrix} 0.80 \\ 0.4 \end{bmatrix}, \begin{bmatrix} 0.85 \\ 0.35 \end{bmatrix}, \begin{bmatrix} 0.9 \\ 0.3 \end{bmatrix}$	$\begin{bmatrix} \text{m} \\ \text{m} \end{bmatrix}$
x_{mic}	$x_d - 0.1$	m

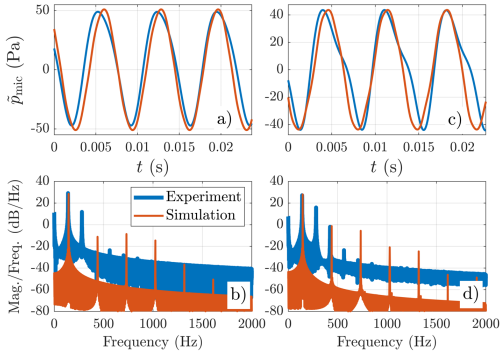


Fig. 3: Open-loop response of the nonlinear Rijke-tube model and the Rijke-tube experiment at the University of Michigan. The experiment's microphone was calibrated to obtain the pressure measurements in pascals (Pa). The parameters used for the model are shown in Table I. a) and b) show the results for $x_d = 0.80$ m and $x_u = 0.40$ m, and c) and d) show the results for $x_d = 0.90$ m and $x_u = 0.30$ m. In all cases, $x_{\text{mic}} = x_d - 0.1$ m. a) and b) show the \bar{p}_{mic} versus time plots of the model and experiment responses. c) and d) show the spectral densities of the model and experiment responses.

where $k \geq 0$ is the controller step, $z_k \in \mathbb{R}^{l_z}$ is the adaptation variable (controller input), for $i = 1, \dots, l_c$, $P_{i,k} \in \mathbb{R}^{l_u \times l_u}$ and $Q_{i,k} \in \mathbb{R}^{l_u \times l_z}$ are the controller coefficient matrices, l_z is the controller input size, l_u is the controller output size, and l_c is the controller-window length. The controller (12) can be written as $u_k = \phi_k \theta_k$, where

$$\phi_k \triangleq [u_{k-1}^T \cdots u_{k-l_c}^T \ z_{k-1}^T \cdots z_{k-l_c}^T] \otimes I_{l_u} \in \mathbb{R}^{l_u \times l_\theta}, \quad (13)$$

$$\theta_k \triangleq \text{vec} [P_{1,k} \cdots P_{l_c,k} \ Q_{1,k} \cdots Q_{l_c,k}] \in \mathbb{R}^{l_\theta}, \quad (14)$$

$l_\theta = l_c l_u (l_u + l_z)$, and θ_k is the vector of controller coefficients to be optimized. If z_k and u_k are scalar signals, then the controller is the SISO transfer function from z_k to u_k given by

$$G_{c,k}(\mathbf{q}) = \frac{Q_{1,k} \mathbf{q}^{l_c-1} + \cdots + Q_{l_c,k}}{\mathbf{q}^{l_c} - P_{1,k} \mathbf{q}^{l_c-1} - \cdots - P_{l_c,k}}, \quad (15)$$

where \mathbf{q} is the time-domain forward-shift operator.

Next, define the retrospective cost variable

$$\hat{z}_k(\hat{\theta}) \triangleq z_k - G_f(\mathbf{q})(u_k - \phi_k \hat{\theta}), \quad (16)$$

where \hat{z}_k is the retrospective-cost variable and $\hat{\theta} \in \mathbb{R}^{l_\theta}$ is the controller coefficient vector determined by optimization below. The rationale underlying (16) is to replace the applied past control inputs with re-optimized control inputs $\phi_k \hat{\theta}$ [26].

The $n_z \times n_u$ finite-impulse-response filter G_f of window length n_f has the form

$$G_f(\mathbf{q}) \triangleq \sum_{i=1}^{n_f} N_i \mathbf{q}^{-i}, \quad (17)$$

where N_1, \dots, N_{n_f} are $l_z \times l_u$ matrices. We can rewrite (16) as $\hat{z}_k(\hat{\theta}) = z_k - N(\bar{U}_k - \bar{\phi}_k \hat{\theta})$, where

$$\bar{\phi}_k \triangleq \begin{bmatrix} \phi_{k-1} \\ \vdots \\ \phi_{k-n_f} \end{bmatrix} \in \mathbb{R}^{n_f l_u \times l_\theta}, \quad \bar{U}_k \triangleq \begin{bmatrix} u_{k-1} \\ \vdots \\ u_{k-n_f} \end{bmatrix} \in \mathbb{R}^{n_f l_u}, \quad (18)$$

$$N \triangleq [N_1 \ \cdots \ N_{n_f}] \in \mathbb{R}^{l_z \times n_f l_u}. \quad (19)$$

All required modeling information is captured by the choice of N . For SISO systems, this information includes the sign of the leading numerator coefficient and nonminimum-phase zeros, if any are present in the sampled-data dynamics [26]. Using $\hat{z}_k(\hat{\theta})$ defined by (16), we define the retrospective cost function

$$J_k(\hat{\theta}) \triangleq \sum_{i=0}^k [\hat{z}_i^T(\hat{\theta}) \hat{z}_i(\hat{\theta}) + (\phi_i \hat{\theta})^T R_u \phi_i \hat{\theta}] + (\hat{\theta} - \theta_0)^T P_0^{-1} (\hat{\theta} - \theta_0), \quad (20)$$

where $P_0 \in \mathbb{R}^{l_\theta \times l_\theta}$ is positive definite and $R_u \in \mathbb{R}^{l_u \times l_u}$ is positive semidefinite. The following result uses recursive least squares to minimize (20); the minimizer $\hat{\theta}_{\min}$ of (20) is used to update the controller coefficient vector θ_k , that is, $\theta_{k+1} \triangleq \hat{\theta}_{\min}$.

Proposition: Let P_0 and R_u be positive definite. Then, for all $k \geq 0$, the retrospective cost function (20) has the unique global minimizer θ_{k+1} given by

$$P_{k+1} = P_k - P_k \begin{bmatrix} N \bar{\phi}_k \\ \phi_k \end{bmatrix}^T \gamma_k \begin{bmatrix} N \bar{\phi}_k \\ \phi_k \end{bmatrix} P_k, \quad (21)$$

$$\theta_{k+1} = \theta_k - P_{k+1} \begin{bmatrix} N \bar{\phi}_k \\ \phi_k \end{bmatrix}^T \bar{R} \begin{bmatrix} z_k - N(\bar{U}_k - \bar{\phi}_k \hat{\theta}) \\ \phi_k \theta_k \end{bmatrix}, \quad (22)$$

where

$$\gamma_k^{-1} \triangleq \bar{R}^{-1} + \begin{bmatrix} N \bar{\phi}_k \\ \phi_k \end{bmatrix} P_k \begin{bmatrix} N \bar{\phi}_k \\ \phi_k \end{bmatrix}^T \in \mathbb{R}^{(l_z+l_u) \times (l_z+l_u)}, \quad (23)$$

$$\bar{R} \triangleq \text{diag}(I_{l_z}, R_u) \in \mathbb{R}^{(l_z+l_u) \times (l_z+l_u)}. \quad (24)$$

For all of the numerical examples and physical tests below, the controller coefficient vector is initialized as $\theta_0 = 0_{l_\theta \times 1}$ in order to reflect the absence of additional prior modeling information. The matrices P_0 and R_u have the form $P_0 = p_0 I_{l_\theta}$ and $R_u = r_u I_{l_u}$, where p_0 and r_u are chosen to tune

the rate of adaptation. Furthermore, for all of the examples in this paper, $l_z = l_u = 1$, and thus all of the controllers are SISO.

Let $e_k \triangleq r_k - y_k$ be the command-following error, where r_k is the sampled command and y_k is the sampled output of the system. The normalized error is defined to be the adaptation variable to improve controller stability. In particular,

$$z_k \triangleq \frac{e_k}{1 + \nu|e_k|}, \quad (25)$$

where ν is the error-normalization parameter, and can be fixed to 0.2.

IV. SAMPLED-DATA IMPLEMENTATION OF THE ADAPTIVE CONTROL LAW

Fig. 4 shows a block diagram of the closed-loop system, where y is the output of the continuous-time system \mathcal{S} and r is the command. The adaptive controller $G_{c,k}$ operates on the sampled error $e_k = r_k - y_k$ and produces the discrete-time control v_k . The controller $G_{c,k}$ and the input v_k are updated at each sampling period $T_s > 0$. The digital-to-analog (D/A) and analog-to-digital (A/D) interfaces considered for this paper are zero-order-hold (ZOH) and sampler, respectively. For this paper, $r \equiv 0$, which reflects the desire to suppress the oscillations in the measured signal, and \mathcal{S} represents the system displayed in Fig. 2 for the numerical examples and the Rijke-tube experiment for the physical tests.

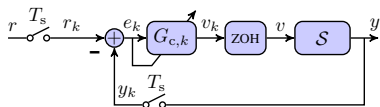


Fig. 4: Adaptive control of a continuous-time system \mathcal{S} .

V. NUMERICAL EXAMPLES USING RIJKE-TUBE MODEL

In this section, the adaptive controller will be used to stabilize the self-excited response of the Rijke-tube model in 2 different cases, in which the heating element is placed at 2 different positions along the tube by changing the positive values of x_d and x_u . Since the length of the tube is 1.2 m in both the model and the experiment, it follows that, for all cases, $x_d + x_u = 1.2$ m. Furthermore, the microphone is always placed 0.1 m below the top of the tube, which implies that $x_{\text{mic}} = x_d - 0.1$ m. As mentioned before, the parameters used for these examples are shown in Table I. In the numerical examples, \mathcal{S} in Fig. 4 is represented by the nonlinear Rijke-tube model, $y = \tilde{p}_{\text{mic}}$, and $r \equiv 0$. The performance of the adaptive controller will be compared against that of the continuous-time, time-delay-integral (TDI) controller used in [31] and represented by the SISO transfer function given by

$$G_{\text{TDI}}(s) = \frac{K_I e^{-\tau_1 s}}{s}, \quad (26)$$

where $K_I \in \mathbb{R}$ and τ_1 is the delay of the controller in seconds. The block diagram that represents the implementation of this controller is shown in Fig. 5.

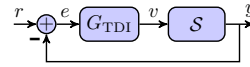


Fig. 5: Continuous-time time-delay integral (TDI) control of a continuous-time system \mathcal{S} .

It will be shown that, while the performance of the TDI controller can degrade under different heating element positions, the adaptive controller is able to adapt and yield similar stabilization performance in all cases, despite lacking prior knowledge of the controlled plant.

The controllers are enabled at $t = 2.5$ s, which is sufficient time for the oscillatory response of all open-loop models to fully develop. For all examples, the RCAC controller parameters are given by $l_c = 5$, $p_0 = 10^{-5}$, $r_u = 1$, $\nu = 0.2$, and $G_f(\mathbf{q}) = -1/\mathbf{q}$, such that $n_f = 1$ and $N = N_1 = -1$. The sampling period for the adaptive controller is $T_s = 0.001$ s. The TDI controller parameters are given by $K_I = 100$ and $\tau_1 = 3.5 \cdot 10^{-3}$ s. For all numerical examples, fixed-step integration is used with step size 10^{-4} s.

Example V-A: $x_d = 0.80$ m, $x_u = 0.40$ m.

Fig. 6 shows the open-loop and closed-loop responses of the Rijke-tube model for the TDI and the RCAC controllers and Fig. 7 shows the controllers' response and the adaptation of the controller coefficients of RCAC. Figs. 6 (a)-(c) show the suppression of the open-loop output oscillations using the TDI and RCAC controllers. Fig. 6 (d) shows that the adaptive controller suppresses the high-magnitude low-frequency content of the open-loop response. \diamond

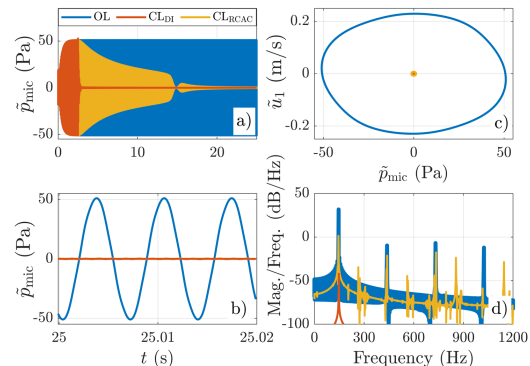


Fig. 6: Example V-A: Adaptive stabilization of the nonlinear Rijke-tube model. a) and b) show the \tilde{p}_{mic} versus time plots of the open-loop (blue), closed-loop with the TDI controller (orange), and closed-loop with the RCAC controller (yellow) responses for $t \in [0, 25]$ s and $t \in [25, 25.02]$ s, respectively. c) shows the \tilde{u}_1 versus \tilde{p}_{mic} plots of the open-loop and closed-loop responses for $t \in [25, 25.02]$ s. d) shows the power spectral densities of the open-loop and closed-loop responses for $t \in [30, 50]$ s.

Example V-B: $x_d = 0.85$ m, $x_u = 0.35$ m.

Fig. 8 shows the open-loop and closed-loop responses of the Rijke-tube model for the TDI and the RCAC controllers and Fig. 9 shows the controllers' response and the adaptation of the controller coefficients of RCAC. Figs. 8 (a)-(c) show an asymptotic output amplitude reduction for the TDI controller and the suppression of the open-loop output

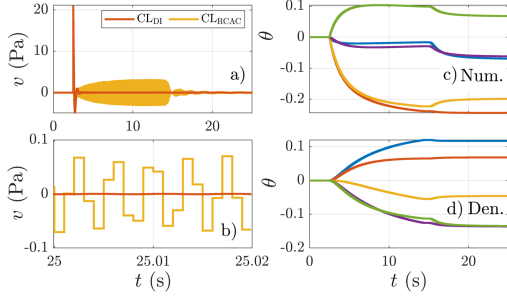


Fig. 7: Example V-A: Controller response and adaptation. *a)* and *b)* show the applied control for $t \in [0, 25]$ s and $t \in [25, 25.02]$ s, respectively, using the TDI controller (orange), and the RCAC controller (yellow). *c)* and *d)* show the evolution of the adaptive controller numerator and denominator coefficients, respectively, for $t \in [0, 25]$ s.

oscillations using the RCAC controller. Fig. 8 (d) shows that the adaptive controller suppresses the high-magnitude low-frequency content of the open-loop response. \diamond

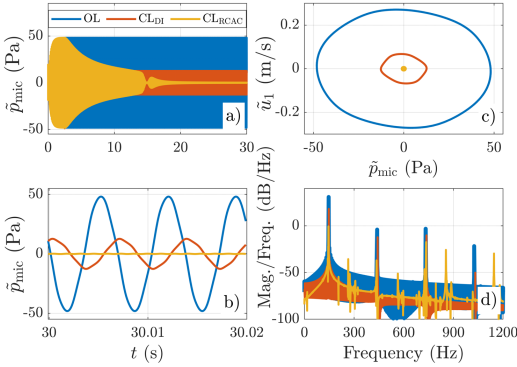


Fig. 8: Example V-B: Adaptive stabilization of the nonlinear Rijke-tube model. *a)* and *b)* show the \tilde{p}_{mic} versus time plots of the open-loop (blue), closed-loop with the TDI controller (orange), and closed-loop with the RCAC controller (yellow) responses for $t \in [0, 30]$ s and $t \in [30, 30.02]$ s, respectively. *c)* shows the \tilde{u}_1 versus \tilde{p}_{mic} plots of the open-loop and closed-loop responses for $t \in [30, 30.02]$ s. *d)* shows the power spectral densities of the open-loop and closed-loop responses for $t \in [30, 50]$ s.

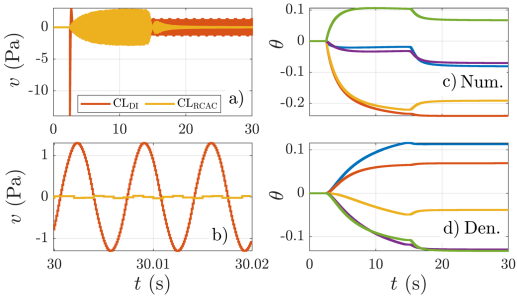


Fig. 9: Example V-B: Controller response and adaptation. *a)* and *b)* show the applied control for $t \in [0, 30]$ s and $t \in [30, 30.02]$ s, respectively, using the TDI controller (orange), and the RCAC controller (yellow). *c)* and *d)* show the evolution of the adaptive controller numerator and denominator coefficients, respectively, for $t \in [0, 30]$ s.

VI. RIJKE TUBE EXPERIMENTAL SETUP

The setup of the Rijke-tube experiment built at the at University of Michigan laboratory is shown in Fig. 10. The heating element is a coil made from 22 gauge nichrome wire with an electrical resistance of approximately 20 ohms. A variac is used as a power supply to heat the coil. A lavalier

microphone is placed at the top of the tube and connected to a preamplifier. The amplified microphone signal is then measured by the Scalexio digital controller via an Analog-to-Digital Converter (ADC). The digital controller implements RCAC and processes the amplified microphone signal to produce an output signal, which is converted to an analog signal via a Digital-to-Analog Converter (DAC). This analog signal is then amplified and used to modulate the speaker. As mentioned in Sec. II, thermoacoustic oscillations will be induced by the heat inside the tube if enough power is provided to the coil.

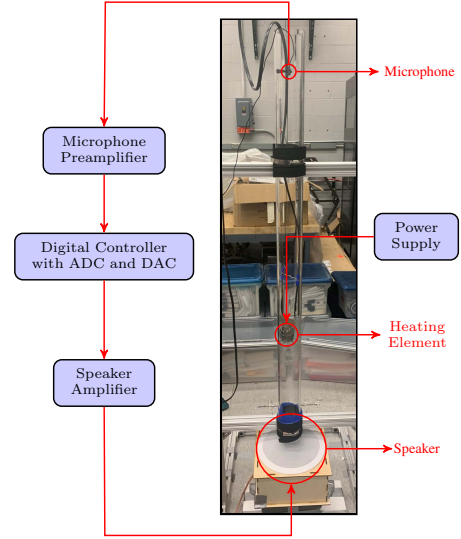


Fig. 10: Rijke-tube experiment at University of Michigan laboratory.

VII. RIJKE TUBE EXPERIMENTAL RESULTS

The setup of the Rijke-tube experiment for the test is similar to that of Example V-A, that is, the coil is placed at approximately 0.40 m from the bottom of the tube and the power provided by the coil is approximately 180 W. RCAC is implemented in the digital controller with the same parameters as in the numerical examples in Sec. V and the same sampling period of $T_s = 0.001$ s. Fig. 11 shows the closed-loop response of the Rijke-tube experiment for the RCAC controller. Fig. 11 (a) shows the suppression of the Rijke-tube experiment output oscillations.

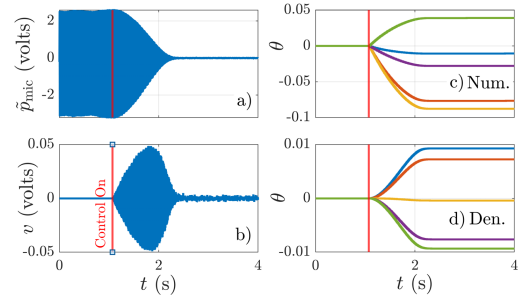


Fig. 11: Adaptive stabilization of Rijke-tube Experiment displayed in Fig. 10. The vertical red line indicates the time at which RCAC starts adapting. *a)* shows the \tilde{p}_{mic} in volts versus time plot of the closed-loop system with the RCAC controller. *b)* shows the control applied by the RCAC controller in volts. *c)* and *d)* show the evolution of the adaptive controller numerator and denominator coefficients, respectively.

VIII. CONCLUSIONS

This paper presented a 1D nonlinear Rijke-tube model, which displays self-excited oscillations, and its open-loop response was compared to that of the Rijke-tube experiment shown in Fig. 10. It was shown numerically that the oscillatory response of the Rijke-tube model can be suppressed using adaptive control implemented in a sampled-data feedback loop. The performance of the adaptive controller was shown to be consistent in all the studied cases, despite lacking prior knowledge of the controlled plant, while the performance of the continuous-time, time-delay-integral controller was shown to degrade under slight changes in model parameters. The numerical results were validated by using the adaptive controller to suppress the oscillatory response of the Rijke-tube experiment shown in Fig. 10. Future work will apply the approach of [32] to the Rijke tube experiment, where G_f is updated online.

IX. ACKNOWLEDGMENTS

This research was supported by NSF grant CMMI 1634709.

REFERENCES

- [1] B. Chance, E. K. Pye, A. K. Ghosh, and B. Hess, Eds., *Biological and Biochemical Oscillators*. Academic Press, 1973.
- [2] P. Gray and S. K. Scott, *Chemical Oscillations and Instabilities: Non-linear Chemical Kinetics*. Oxford, 1990.
- [3] A. Goldbeter and M. J. Berridge, *Biochemical Oscillations and Cellular Rhythms: The Molecular Bases of Periodic and Chaotic Behaviour*. Cambridge, 1996.
- [4] Y. Chen and J. F. Driscoll, "A multi-chamber model of combustion instabilities and its assessment using kilohertz laser diagnostics in a gas turbine model combustor," *Comb. Flame*, vol. 174, pp. 120 – 137, 2016.
- [5] E. Awad and F. E. C. Culick, "On the existence and stability of limit cycles for longitudinal acoustic modes in a combustion chamber," *Comb. Sci. Tech.*, vol. 46, pp. 195 – 222, 1986.
- [6] A. Jenkins, "Self-oscillation," *Phys. Rep.*, vol. 525, no. 2, pp. 167 – 222, 2013.
- [7] W. Ding, *Self-Excited Vibration: Theory, Paradigms, and Research Methods*. Springer, 2010.
- [8] E. Jonsson, C. Risoa, C. A. Luppa, C. E. S. Cesnik, J. R. R. A. Martins, and B. I. Epureanu, "Flutter and post-flutter constraints in aircraft design optimization," *Prog. Aerosp. Sci.*, vol. 109, 2019, article 100537, 28 pages.
- [9] B. D. Coller and P. A. Chamara, "Structural non-linearities and the nature of the classic flutter instability," *J. Sound Vibr.*, vol. 277, pp. 711–739, 2004.
- [10] P. P. Friedmann, "Renaissance of aeroelasticity and its future," *J. Aircraft*, vol. 36, pp. 105–121, 1999.
- [11] A. P. Dowling and A. S. Morgans, "Feedback control of combustion oscillations," *Annu. Rev. Fluid Mech.*, vol. 37, pp. 151–182, 2005.
- [12] T. Yi and E. J. Gutmark, "Adaptive control of combustion instability based on dominant acoustic modes reconstruction," *Comb. Sci. Tech.*, vol. 180, no. 2, pp. 249–263, 2007.
- [13] A. Banaszuk, Y. Zhang, and C. A. Jacobson, "Adaptive control of combustion instability using extremum-seeking," in *Proc. Amer. Contr. Conf.*, 2000, pp. 416–422.
- [14] S. Evesque and A. Dowling, "Adaptive control of combustion oscillations," in *4th AIAA/CEAS Aeroacoustics Conf.*, 1998, p. 2351.
- [15] S. Koshigoe, T. Komatsuzaki, and V. Yang, "Adaptive control of combustion instability with on-line system identification," *J. Prop. and Power*, vol. 15, no. 3, pp. 383–389, 1999.
- [16] G. Billoud, M. Galland, C. Huynh Huu, and S. Cancel E, "Adaptive active control of combustion instabilities," *Comb. Sci. Tech.*, vol. 81, no. 4-6, pp. 257–283, 1992.
- [17] J. P. Epperlein, B. Bamieh, and K. J. Astrom, "Thermoacoustics and the Rijke tube: Experiments, identification, and modeling," *IEEE Contr. Sys. Mag.*, vol. 35, no. 2, pp. 57–77, 2015.
- [18] K. Balasubramanian and R. Sujith, "Thermoacoustic instability in a Rijke tube: Non-normality and nonlinearity," *Phys. Fluids*, vol. 20, no. 4, 2008.
- [19] M. A. Heckl, "Active control of the noise from a Rijke tube," *J. Sound Vibr.*, vol. 124, no. 1, pp. 117–133, 1988.
- [20] —, "Non-linear acoustic effects in the Rijke tube," *Acta Acust. united Ac.*, vol. 72, no. 1, pp. 63–71, 1990.
- [21] W. Wei, J. Wang, D.-h. Li, M. Zhu, H.-j. Tang, and F.-l. Weng, "Dynamic compensation based adaptive control of thermo-acoustic instabilities in Rijke tube: An experimental validation," *ISA Trans.*, vol. 52, no. 3, pp. 450–460, 2013.
- [22] J. Rubio-Hervas, M. Reyhanoglu, and W. MacKunis, "Observer-based sliding mode control of Rijke-type combustion instability," *J. Low Freq. Noise, Vibr., Active Contr.*, vol. 34, no. 2, pp. 201–217, 2015.
- [23] R. Blombou, A. Laverdant, S. Zaleski, and P. Kuentzmann, "Active control of combustion instabilities on a Rijke tube using neural networks," *Proc. Comb. Inst.*, vol. 28, no. 1, pp. 747–755, 2000.
- [24] M. A. Vaudrey, W. T. Baumann, and W. R. Saunders, "Time-averaged gradient control of thermoacoustic instabilities," *J. Prop. and Power*, vol. 19, no. 5, pp. 830–836, 2003.
- [25] A. S. Morgans and A. M. Annaswamy, "Adaptive control of combustion instabilities for combustion systems with right-half plane zeros," *Comb. Sci. Tech.*, vol. 180, no. 9, pp. 1549–1571, 2008.
- [26] Y. Rahman, A. Xie, and D. S. Bernstein, "Retrospective Cost Adaptive Control: Pole Placement, Frequency Response, and Connections with LQG Control," *IEEE Contr. Sys. Mag.*, vol. 37, pp. 28–69, Oct. 2017.
- [27] A. Goel, A. Xie, K. Duraisamy, and D. S. Bernstein, "Retrospective Cost Adaptive Thrust Control of a 1D Scramjet with Mach Number Disturbance," in *Proc. Amer. Contr. Conf.*, Chicago, IL, July 2015, pp. 5551–5556.
- [28] A. Goel, K. Duraisamy, and D. S. Bernstein, "Retrospective cost adaptive control of unstart in a model scramjet combustor," *AIAA J.*, vol. 56, no. 3, pp. 1085–1096, 2018.
- [29] A. P. Dowling, "Nonlinear Self-Excited Oscillations of a Ducted Flame," *J. Fluid Mech.*, vol. 346, pp. 271–291, 1997.
- [30] N. Olgac, U. Zalluhoglu, and A. S. Kammer, "Predicting thermoacoustic instability: a novel analytical approach and its experimental validation," *J. Prop. and Power*, vol. 30, no. 4, pp. 1005–1015, 2014.
- [31] U. Zalluhoglu, A. S. Kammer, and N. Olgac, "Delayed feedback control laws for Rijke tube thermoacoustic instability, synthesis, and experimental validation," *IEEE Trans. Contr. Sys. Tech.*, vol. 24, no. 5, pp. 1861–1868, 2016.
- [32] S. A. U. Islam, T. Nguyen, I. Kolmanovsky, and D. S. Bernstein, "Data-Driven Retrospective Cost Adaptive Control for Flight Control Applications," *J. Guid. Contr. Dyn.*, vol. 44, pp. 1732–1758, October 2021.